Generation of Internal Solitary Waves by Lateral Circulation in a Stratified Estuary

XIAOHUI XIE AND MING LI

Horn Point Lab, University of Maryland Center for Environmental Science, Cambridge, Maryland

MALCOLM SCULLY

Department of Applied Ocean Physics and Engineering, Woods Hole Oceanographic Institution, Woods Hole, Massachusetts

WILLIAM C. BOICOURT

Horn Point Lab, University of Maryland Center for Environmental Science, Cambridge, Maryland

ABSTRACT

Internal solitary waves are commonly observed in the coastal ocean where they are known to contribute to mass transport and turbulent mixing. While these waves are often generated by cross-isobath barotropic tidal currents, novel observations are presented suggesting that internal solitary waves result from along-isobath tidal flows over channel-shoal bathymetry. Mooring and ship-based velocity, temperature, and salinity data were collected over a cross-channel section in a stratified estuary. The data show that Ekman forcing on along-channel tidal currents drives lateral circulation, which interacts with the stratified water over the deep channel to generate a supercritical mode-2 internal lee wave. This lee wave propagates onto the shallow shoal and evolves into a group of internal solitary waves of elevation due to nonlinear steepening. These observations highlight the potential importance of three-dimensionality on the conversion of tidal flow to internal waves in the rotating ocean.

1. Introduction

Internal solitary waves (ISWs hereinafter) are ubiquitous in the stratified coastal ocean and play an important role in generating turbulent mixing (e.g., Moum et al. 2003; MacKinnon and Gregg 2003; Klymak and Moum 2003; Alford et al. 2012) and transporting sediments (Bogucki et al. 1997; Hosegood and van Haren 2004) and biochemically important materials (Pineda 1991; Omand et al. 2011). They mainly originate from barotropic tidal currents over abrupt topography such as shelf breaks (Holloway 1987; Gerkema and Zimmerman 1995; Xie et al. 2015), banks (Scotti et al. 2007), and sills (Farmer and Armi 1999; Cummins et al. 2003). In a pioneering study, Maxworthy (1979) showed that a large pycnocline depression is generated downstream of a sill when strong tidal flows pass over the sill. As the tide slackens, the depression moves upstream and decomposes into a group of rank-ordered solitary waves.

In most studies of internal wave generation by flow–topography interaction, a two-dimensional flow is often assumed (Melville and Helfrich 1987; Cummins et al. 2006; Helfrich and Melville 2006; Jackson et al. 2012). As a result, internal wave generation is attributed to vertical motions caused by cross-isobath tidal flows, while along-isobath tidal flows are not expected to generate internal wave motions. It is well known that along-isobath flows over a sloping bottom generate cross-isobath (lateral) Ekman transport under certain conditions (Garrett et al. 1993). This is especially true in a strait (Martin et al. 2005) or an estuary (Lerczak and Geyer 2004). Although lateral currents associated with along-isobath flows over a sloping bottom are known to generate vertical motions (Garrett et al. 1993; Martin et al. 2005), they have not been linked to the generation of large-amplitude internal waves. In this paper, we report such observations in a stratified estuary, suggesting that ISWs can be generated from lateral circulation over channel-shoal bathymetry.
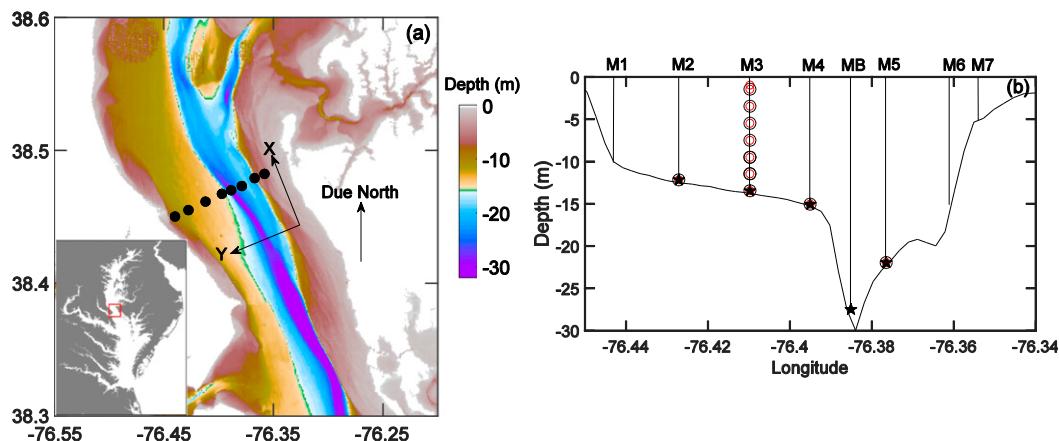
FIG. 1. (a) Map showing bathymetry and eight mooring sites (filled circles) in the middle of Chesapeake Bay as indicated by the red rectangle in the inset map. The x and y axes represent the along-channel and cross-channel directions. (b) The cross-channel section and mooring locations. Black stars, black circles, and red circles mark the locations of ADCPs, ADVs, and TC sensors, respectively.

2. Field observations and methods

Chesapeake Bay is located in the Mid-Atlantic region of the United States (Fig. 1a). Like many coastal plain estuaries, Chesapeake Bay features channel-shore bathymetry (Dyer 1998). A deep channel with a maximum depth of 40–50 m runs approximately along the center axis of the estuary and is flanked by two shallow shoals with depths of 5–15 m.

A field campaign was conducted in Chesapeake Bay between 22 August and 31 October 2013. A cross-channel mooring array, consisting of eight moorings, was deployed in a relatively straight section of the estuary (Fig. 1a). It provided continuous measurements of currents, temperature, and conductivity over the 2-month period. Our analysis focuses on the data obtained from the five mooring stations M2–M5 and MB (Fig. 1b), in order to capture the generation of internal waves at the edge of the deep channel and their subsequent propagation over the shallow western shoal. Mooring stations M2 and M3 were located on the western shoal, M4 sat at the edge of the western shoal, MB was deployed in the deep channel, and M5 was located on the eastern edge of the channel.

Each mooring at M2–M4 was equipped with a bottom-mounted (1200 KHz) acoustic Doppler current profiler (ADCP), a Nortek vector acoustic Doppler velocimeter (ADV), and a temperature-conductivity (TC) sensor. The TC sensors collected a sample every 5 min. The 8-MHz ADV at the M3 site sampled at 32 Hz and collected 28 min of data every 30 min, while the 5-MHz ADVs at the M2 and M4 sites sampled at 25 Hz and collected 5 min of data every 30 min. At MB and M5, a 600-KHz bottom-mounted ADCP was deployed. All

ADCPs sent an acoustic ping every 1 s to measure velocity profiles and recorded the average over 300-s intervals (30-s intervals at M3). They had a vertical resolution of 0.5 m (M2 and M4) or 1 m (M3, MB, and M5). In addition, a fixed tower was deployed close to the M3 mooring (~50 m to the south), with continuous measurements between 18 September and 29 October (Scully et al. 2015). The tower contained a vertical array of six Nortek 8-MHz ADVs sampling at 32 Hz and six Seabird SBE37 microcat CTDs collecting a sample every 5 min. They occupied a depth range of 1.5–11.5 m with a vertical resolution of 2 m. The tower was also equipped with a vertical array of 12 RBR solo-T thermistors, measuring temperature at depths of 1.5–12.5 m at a sampling rate of 1 Hz and a vertical spacing of 1 m. Details of the tower deployments are described in Scully et al. (2015).

Velocities measured by the ADCPs are rotated into the along-channel (x), across-channel (y), and vertical (z) components (u, v, w) based on the major axis of the depth-averaged tidal flows. The principal flow directions at the M2–M5 sites are within 10° of each other and are averaged to define the x direction, which is approximately aligned with the isobaths (Fig. 1a). The positive x and y directions are defined as 340°N and 250°N, measured clockwise from the true north direction. For simplicity, the positive x direction is called northward and the positive y direction is called westward. The ADCPs have relatively low temporal resolutions and cannot resolve high-frequency internal waves in the estuary. Instead, they are used to characterize mean flows such as tidal currents and lateral circulation. A third-order Butterworth low-pass filter with a cutoff frequency of 1 h is used to remove high-frequency signals in the ADCP data.

High-resolution RBR and ADV data are used to identify high-frequency internal waves. The ADV data
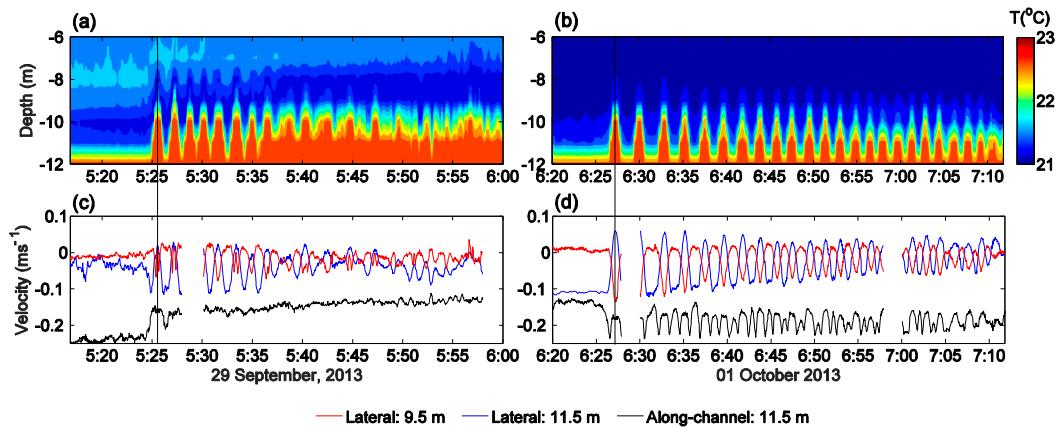
FIG. 2. Time–depth distributions of high-frequency temperature fluctuations at the tower/M3 on (a) 29 September and (b) 1 October. (c),(d) Along-channel (black) and lateral (blue) velocities obtained from an ADV deployed at a depth of 11.5 m during the same two periods. Also shown is the lateral velocity at 9.5 m depth (red). The vertical black line indicates the crest of the first wave in the ISW packet.

are averaged over a 1-s interval yielding 1 Hz data, at the same temporal resolution as the RBR data. A high-pass Butterworth filter with a cutoff frequency of 10 min is applied to the ADV data when estimating the propagation direction of ISWs.

3. Results

a. Observations of internal solitary waves

High-frequency temperature and velocity data collected at the tower revealed frequent occurrences of ISWs. Two representative internal wave trains are shown in Fig. 2. They had periods of 1–3 min and lasted for 0.5–2 h. Since the water column was well mixed in the top 11 m and stratified in the bottom 3 m at the tower's location, the waves were trapped near the sea bed. The vertical isotherm displacements induced by the waves were 1–3 m (Figs. 2a,b). The waves exhibited the shape of ISWs of elevation. They induced a velocity anomaly consistent with a mode-1 wave structure: the westward velocity anomaly at a depth of 11.5 m has a sign opposite to that at a depth of 9.5 m (Figs. 2c,d). The largest westward velocity anomaly was observed at the depth of 13.8 m (~0.7 m above the seafloor), while the waves decayed rapidly above the depth of 9.5 m due to weak stratification, with strong damping of the velocity anomaly (not shown).

The along-channel velocity anomaly associated with internal waves was much smaller than the lateral velocity anomaly (Figs. 2c,d), suggesting that these waves may have propagated primarily in the cross-channel direction. For an ISW of elevation (depression) in a two-layer fluid, the wave-induced horizontal velocity in the lower (upper) layer is the same as the wave propagation direction with respect to the background flow (Xie et al.

2015). The westward bottom velocity anomaly in the lower layer implies that the ISWs propagated westward. To determine the propagation direction θ of ISWs more precisely, we use the filtering method described in Mirshak and Kelley (2009):

$$\theta = \arctan(v'/u'), \qquad (1)$$

where v' and u' are the cross-channel (y direction) and along-channel (x direction) velocity anomalies induced by ISWs. We use the velocities measured at the depth of 13.8 m where the wave-induced isopycnal displacements were small but the velocity anomalies were strongest. ADV measurements at 11.5 m depth (close to pycnocline) are not used because wave heaving of the background flow sometimes causes large biases in the estimate of θ, as illustrated by Mirshak and Kelley (2009) and Xie et al. (2015). Figure 3 shows the inferred wave propagation direction for the ISW observed between 26 September and 2 October, during which the ISW trains appeared roughly every 12 h at the M3 mooring site (see Fig. 6a for a detailed discussion). To find θ for each wave packet, we select ISWs whose velocity magnitude ($\sqrt{v'^2 + u'^2}$) is greater than 0.1 m s^{-1} and obtain an average value of θ. All the wave packets propagated in a westward direction that was within ±20° of the cross-channel direction.

This westward propagation of the ISWs is also seen clearly in a comparison of the lateral velocity time series at the M4, M3, and M2 mooring stations on 1 October (Fig. 4a). Between 0620 and 0830 local standard time (LST), a westward bottom velocity anomaly was observed at M3. High-frequency velocity oscillations, indicative of an ISW train, were superposed on the forward face of this westward velocity anomaly (between 0620 and 0700 LST). This ISW train could not be traced back
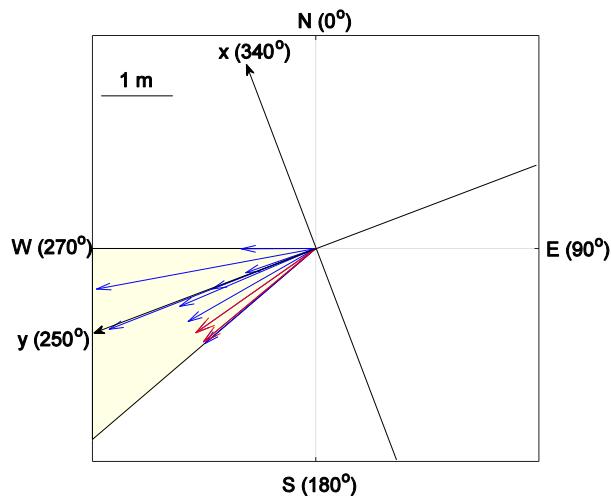
FIG. 3. The propagating direction of ISW packets observed at M3 between 26 September and 2 October. The length of an arrow indicates the largest isopycnal displacement in each wave packet. Two cases shown in Fig. 2 are highlighted by red arrows. The shaded region indicates ±20° around the positive y axis.

to the M4 site located at the edge of the deep channel. However, a low-frequency westward velocity anomaly was observed at M4 between 0500 and 0700 LST. In contrast, the lateral velocity at M2 showed large-amplitude, high-frequency fluctuations lasting from 0815 to 1015 LST. It appears that the ISW train moving past M3 over a period of 40 min transformed into an ISW train with larger amplitudes and longer duration (~2 h) at M2. It took approximately 2 h for the ISWs to travel from M3 (0620 LST) to M2 (0820 LST), corresponding to a westward wave propagation speed of ~0.2 m s^{-1}.

b. Observations of lateral circulation

The ISW trains appeared roughly every 12 h at the M3 mooring site between 25 September and 2 October, pointing to a tidal connection. Since the ISWs primarily propagated in the lateral direction, they may result from the interactions between tidally driven lateral currents and channel-shoal bathymetry. Like stratified flows over a sill or undersea valley (Maxworthy 1979; Farmer and Armi 1999; Wang 2006), it is possible that lateral currents advecting stratified water over the deep channel generate internal lee waves that subsequently propagate onto the shallow shoal and evolve into ISWs through nonlinear steepening.

Lateral or transverse circulation has been widely reported in estuaries (e.g., Nunes and Simpson 1985; Huijts et al. 2009). It can feature two counterrotating cells driven by differential advection (Lerczak and Geyer 2004) or one cell circulation driven by lateral Ekman forcing (Scully et al. 2009). In a numerical modeling study, Li et al. (2014) showed that lateral circulation switches from two-cell circulation in narrow estuaries to one-cell circulation in wide estuaries. If the Kelvin number, defined as

$$\mathrm{Ke} = \frac{fB}{\sqrt{g'h_s}} \qquad (2)$$

in which f is the Coriolis parameter, B is the estuary width, g' is the reduced gravitational acceleration determined by the density difference between the upper and lower layers, and h_s is the mean depth of the upper layer, exceeds ~0.1, the lateral circulation consists of
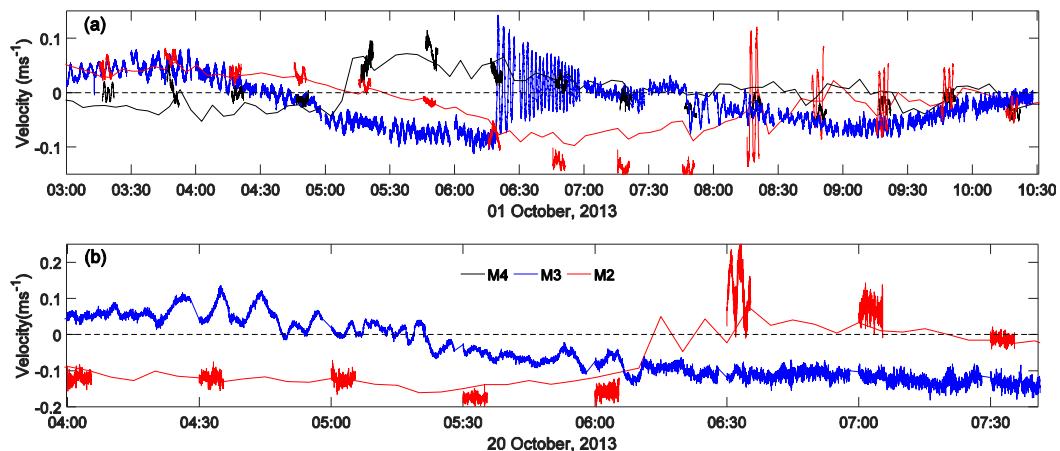

FIG. 4. Time series of lateral velocities at M4 (black), M3 (blue), and M2 (red) mooring sites on (a) 1 October and (b) 20 October. At M3 a bottom-mounted ADV provided continuous high-frequency velocity measurements. At M2 and M4 moorings, the ADVs only recorded 5 min of measurements every 30 min. The discontinuous ADV time series are complemented by low-frequency ADCP measurements at M4 (14-m depth) and M2 (11-m depth), respectively.
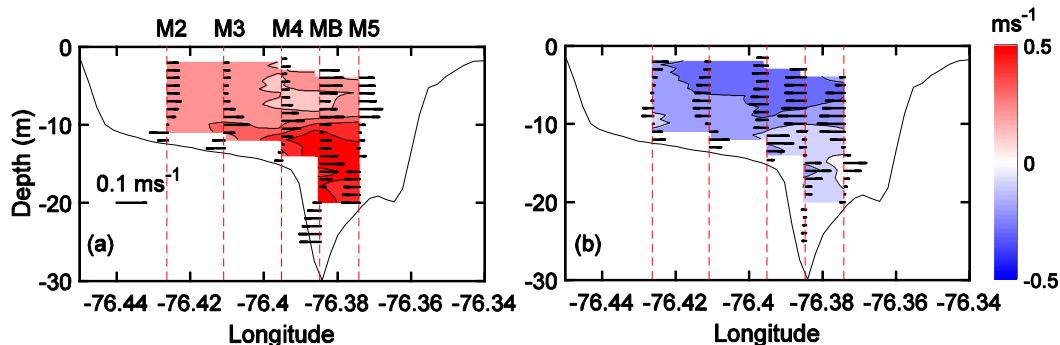
FIG. 5. Cross-channel distributions of the along-channel (color) and lateral (horizontal black lines) velocities during (a) flood and (b) ebb tides, obtained from bottom-mounted ADCPs at the mooring stations.

one rotating cell that switches its sense of rotation over a flood–ebb tidal cycle (Li et al. 2014).

Chesapeake Bay is a wide estuary: Ke ≈ 2.5 during the observational period and exceeds the threshold of ~0.1 above which the lateral Ekman forcing is expected to be a dominant mechanism in driving the lateral circulation (Li et al. 2014). Figure 5 shows two snapshots of the lateral and along-channel velocities obtained from the ADCP measurements at the mooring stations. On the flood tide, a westward current developed in the bottom layer (Fig. 5a), consistent with the Ekman forcing on the landward tidal current, while a return flow developed in the upper layer to form a clockwise circulation (looking into the estuary). On the ebb tide, however, the bottom current was directed eastward and the lateral circulation formed a counterclockwise circulation (Fig. 5b). Note that, under wind-forced conditions, Xie et al. (2017) also observed one-cell lateral circulation in Chesapeake Bay that was driven by lateral Ekman forcing in the surface layer.

The overall strength and the sense of rotation in the lateral circulation can be described by integrating the streamwise vorticity ($\omega_x = -\partial v/\partial x + \partial w/\partial y \approx -\partial v/\partial z$) (see Li et al. 2014) in the cross-channel section using the ADCP measurements at the four moorings (M3, M4, MB and M5). This yields a sectionally averaged streamwise vorticity $\overline{\omega}_x$. As shown in Figs. 6a and 6b, $\overline{\omega}_x$ was mostly positive (clockwise circulation) on flood tides and mostly negative (counterclockwise circulation) on ebb tides. However, there is often a phase difference of 1–2 h between the peak tidal current and maximum lateral circulation strength, as demonstrated in the numerical modeling study of Li et al. (2014).

c. Generation of internal waves by lateral circulation

An internal lee wave was indeed generated over the deep channel, as captured by high-resolution surveys from a towed undulating vehicle (Scanfish) equipped

with a CTD during 19–20 October (Fig. 7; no Scanfish survey conducted between 26 September and 2 October). Five cross-channel transects were conducted near the mooring array over a span of 4 h (Fig. 7a). A mode-2 internal lee wave, with a characteristic bulge between the isopycnals of 11.5 and 12.3 kg m^{-3}, appeared above the deep channel during the second and third transects (Figs. 7c,d). Note that the density plotted in Figs. 7b–f is σ_t and a reference density of 1000 kg m^{-3} is subtracted from the actual density. This lee wave subsequently propagated westward and evolved into a mode-1 wave on the shallow shoal (Figs. 7e,f). At this time, tidal flows were in the ebb direction. The lateral Ekman forcing drove a counterclockwise lateral circulation, with a westward current in the upper mixed layer and an eastward current in the lower stratified layer (see Figs. 7c,d).

We hypothesize that the eastward lateral flows advect stratified water across the western flank of the deep channel, generating the mode-2 internal lee wave. To illustrate this mechanism, we calculate the Froude number $Fr_i = |V/C_i|$, where V is the averaged lateral velocity in the lower stratified water and C_i is the phase speed of the long internal wave of mode i at the edge of the deep channel (at the M4 location). Parameter C_i is found by solving the eigenvalue problem (Gill 1982):

$$\frac{d^2\Phi(z)}{dz^2} + \frac{N^2(z)}{C_i^2}\Phi(z) = 0, \qquad (3)$$

with the boundary conditions $\Phi(0) = \Phi(-h) = 0$, where h is the water depth. The background buoyancy frequency $N(z)$ is calculated from the tidally averaged TC data, and i is the mode number. During the second transect, $Fr_2 = 0.6$ and a mode-2 internal disturbance was generated above the western flank of the deep channel (Fig. 7c). During the third transect, the lateral flows became supercritical ($Fr_2 = 1.5$). As a result, the
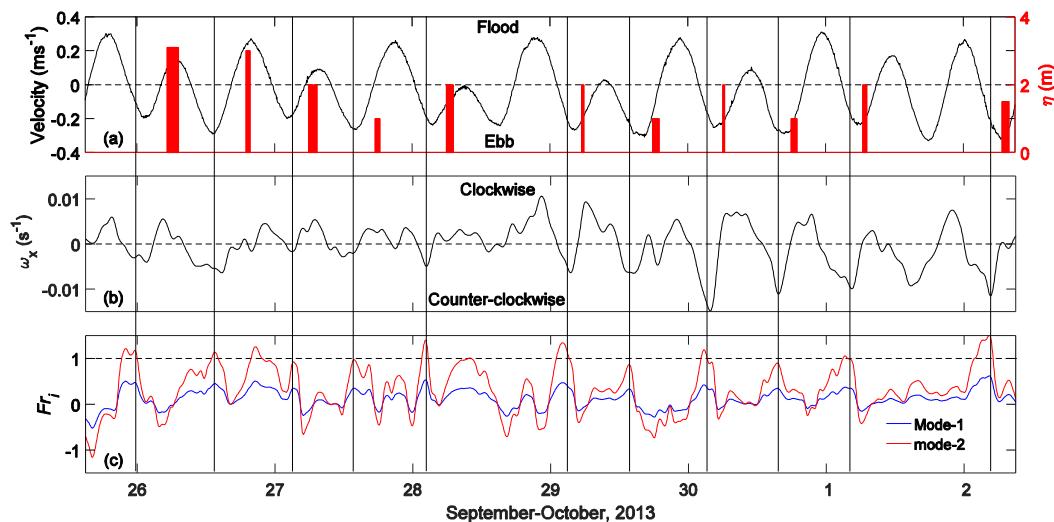
FIG. 6. (a) Time series of the depth-averaged along-channel flow between 25 September and 2 October. The red vertical bars indicate the arrival time and duration of the internal solitary waves observed at the tower. The height of the bars represents the largest vertical displacement in the wave trains. (b) Time series of the sectionally averaged streamwise vorticity $\overline{\omega}_x$, characterizing the overall strength of the lateral circulation (positive/negative for clockwise/counterclockwise circulation). (c) Time series of Fr_1 (blue) and Fr_2 (red) calculated from the velocity at M4 with respect to mode-1 and mode-2 internal waves. Note that Fr_i is defined to be negative for westward velocity. The black vertical solid lines mark the maxima of Fr_i while the horizontal dashed line in (c) indicates the critical value of $Fr_2 = 1$.

internal disturbance grew in amplitude, forming a large lee wave (Fig. 7d). Previous observations (Farmer and Smith 1980) and numerical experiments (da Silva et al. 2015) also showed the generation of large-amplitude mode-2 lee waves in the lee of a sill. As the lateral flow weakened ($Fr_2 < 1$), the mode-2 lee wave propagated onto the western shore (Fig. 7e), transitioning to a mode-1 elevation wave (Fig. 7f). The westward traveling elevation wave would generate a westward velocity anomaly at the bottom, as shown in Fig. 4a. Unlike the two cases shown in Fig. 2, the lee wave in Fig. 7 had not yet evolved into ISWs of elevation when it reached M3 (Fig. 4b). However, large high-frequency lateral velocity oscillations were observed at the shallower M2 site around 0630 LST, indicating the arrival of the ISW train.

Figure 6 summarizes 11 episodes of ISWs that were observed between 25 September and 2 October. The ISWs typically appeared at M3 sometime after lateral circulation began rotating in a counterclockwise direction (during ebb tide) and lateral flow in the lower stratified layer on the western shoal was directed toward the deep channel (cf. Figs. 6a and 6b). Most importantly, the appearances of the ISWs at M3 were almost always preceded by supercritical or nearly critical flows at the edge of the deep channel (M4 mooring site; Fig. 6c). The Froude number Fr_2, with respect to the mode-2 wave, exceeded 1, even though the flow remained subcritical when compared with the phase speed of the mode-1

wave ($Fr_1 < 1$). It is noted that Fr_2 was in the range of 0.85–1 during the two internal wave events on 27 September, one event on 29 September, and one event on 30 September. The observed ISWs during these four events were relatively weak, with a maximum displacement of ~1 m. Small-amplitude lee waves can be generated at these near-critical flows, as shown in Fig. 7c. Maxworthy (1979) also observed lee waves in his laboratory experiment of stratified flows over a sill when the Froude number was between 0.5 and 1. Therefore, the time series analysis of the mooring records is consistent with the story emerging in Fig. 7. A mode-2 internal lee wave was generated on the western flank of the deep channel due to the flow–topography interaction. As the eastward flow weakened, the lee wave propagated westward, transformed into a mode-1 elevation wave on the shallow western shoal, and decomposed into ISWs of elevation.

The above data analysis suggests a novel mechanism for the generation of ISWs in stratified estuaries, as illustrated in the schematic diagram of Fig. 8. During ebb tide, the lateral Ekman transport associated with the along-channel tidal currents produces eastward flows over the western flank of the deep channel associated with a counterclockwise lateral circulation. The eastward flows become supercritical/critical ($Fr_2 \geq 1$) and generate a mode-2 internal lee wave (Fig. 8a). As the lateral circulation weakens, the mode-2 lee wave
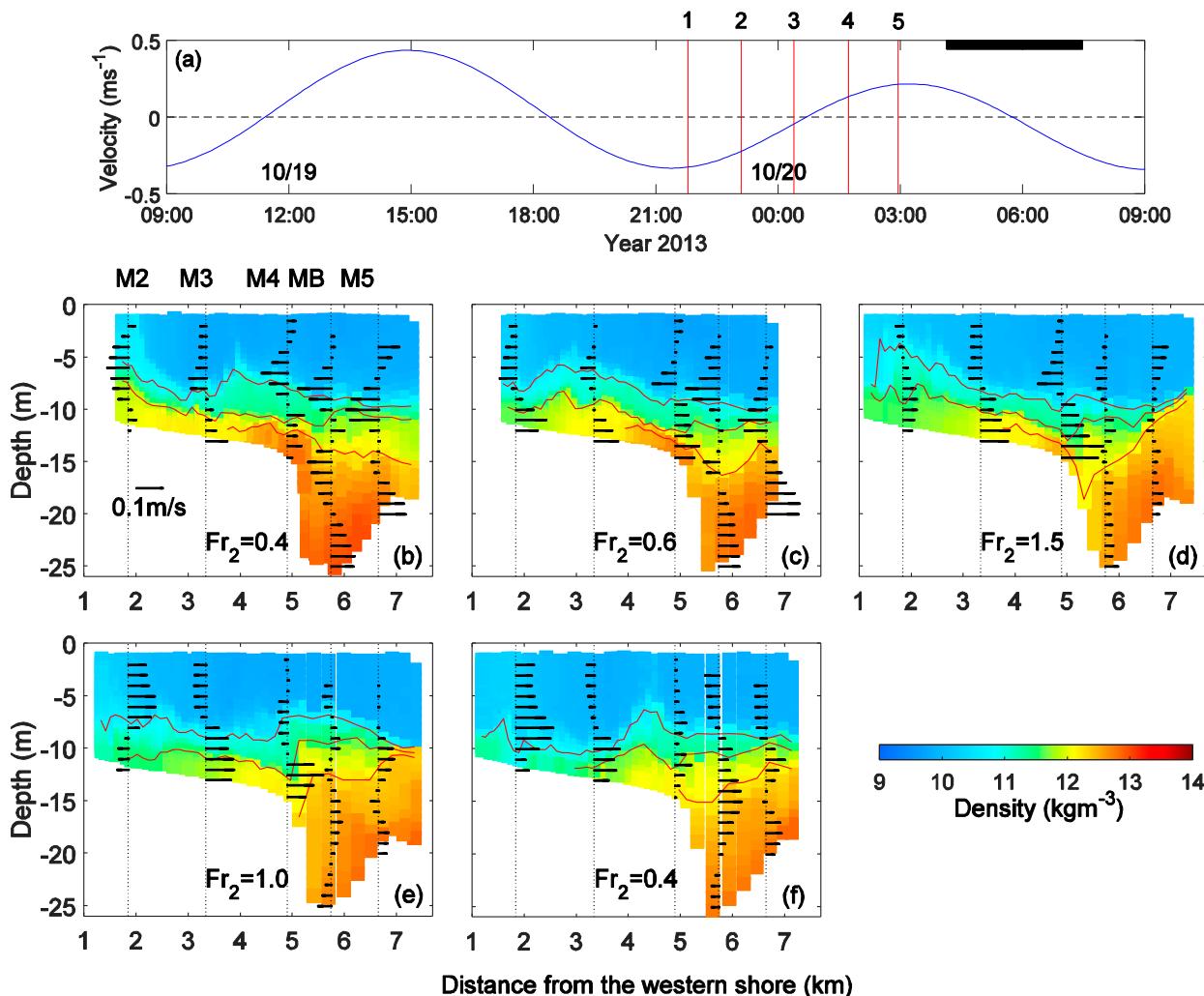
FIG. 7. (a) Time series of the depth-averaged along-channel flow at M4 during 19–20 October 2013. The vertical lines indicate the initialization time of five transect surveys, each of which lasted 30 min. The black rectangle indicates the period in Fig. 4b. (b)–(f) Five transects of high-resolution density field (color) obtained from a ship-towed undulating vehicle, supplemented by lateral velocity measurements (vectors) from bottom-mounted ADCPs at the mooring stations. Red contours highlight isopycnals with density of 10.5, 11.5, and 12.3 $kg\,m^{-3}$. Note that the plotted density is the actual density minus a reference density of 1000 $kg\,m^{-3}$. The value of Froude number Fr_2 is shown for each transect.

propagates westward and evolves into a mode-1 wave of elevation because of its interaction with the two-layer stratification on the western shoal (Fig. 8b). During its westward propagation over the shoaling bottom, the elevation wave is decomposed into a group of ISWs of elevation due to nonlinear steepening (Fig. 8c). The lateral circulation weakens or reverses its sense of rotation as the tide transitions from the ebb to flood phase.

It should be noted that the ISWs were not always observed at exactly the same tidal phase (Fig. 6a). Two factors could have contributed to this phase variation. First, the maximum lateral circulation strength (and the peak value of Fr) varied somewhat between different tidal cycles (Figs. 6a–c). Second, the transit time from the

deep channel to shallow shoal was dependent on stratification in the water column. Between 25 September and 2 October, stratification on the western shoal increased such that the phase speed C_p of the mode-1 (mode-2) internal wave increased from ~0.15 $m\,s^{-1}$ (0.06 $m\,s^{-1}$) on 26 September to ~0.25 $m\,s^{-1}$ (0.1 $m\,s^{-1}$) on 2 October.

4. Conclusions and discussion

We have presented observations of ISWs in a stratified estuary that features channel-shoal bathymetry. These internal waves have vertical isopycnal displacements that are a significant fraction of the water depth and may have important implications for turbulent
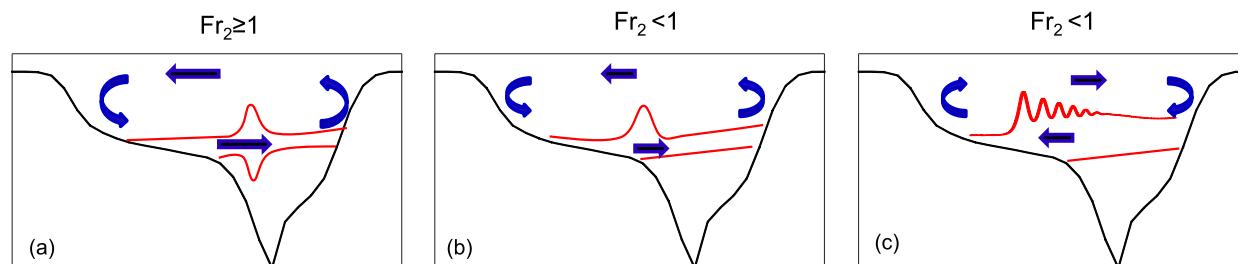
FIG. 8. Schematic depicting the generation of internal solitary waves. (a) The interaction between the lateral circulation and channel-shoal bathymetry generates a mode-2 lee wave, which (b) propagates toward the left as the lateral flow weakens and (c) transitions to mode-1 internal solitary waves through nonlinear steepening over the shallow shoal.

mixing and biogeochemical cycling. Unlike previous assumptions that internal waves are generated by the interaction between cross-isobath tidal flows and topography, we found that ISWs can also be generated by lateral circulation associated with along-isobath tidal flows over channel-shoal topography.

The observed lateral generation mechanism may apply to other coastal environments. For example, observations in the Strait of Juan de Fuca suggested that cross-isobath Ekman transport associated with along-channel tidal currents was essential to generate large vertical isopycnal excursions (Martin et al. 2005). Cross-isobath propagation of ISWs was also observed in the St. Lawrence Estuary (Bourgault et al. 2007) and in the Faeroe–Shetland Channel (Hosegood and van Haren 2004). It is quite possible that these waves were generated by the interaction between the lateral currents and lateral bathymetry change.

Although the observations and data analyses presented in this study are highly suggestive of a lateral wave generation mechanism, we cannot ignore other possible mechanisms. The mooring arrays were located in a relative straight segment of the estuary, but there are still bathymetry variations in the along-channel direction, and changes in the orientation of the channel could result in interactions between along-channel flows and lateral bathymetry. A more extensive field program with mooring stations spanning in both cross-channel and along-channel directions could more precisely pinpoint the wave propagation direction and discern the wave generation mechanism. We could also conduct a high-resolution numerical modeling study of an idealized straight estuarine channel featuring channel-shoal bathymetry and investigate if lateral currents advecting stratified water over the deep channel will generate internal lee waves that propagate onto the shallow shoal and evolve into ISWs.

Acknowledgments. We thank Larry Sanford, Carl Friedrich, Alex Fisher, and other members of our NSF project team for helpful discussions. Carole Derry's assistance in data processing is greatly appreciated. We are grateful to two reviewers for their helpful comments and to the National Science Foundation (OCE-1061609) for the financial support.

REFERENCES

Alford, M. H., J. B. Mickett, S. Zhang, Z. Zhao, and J. Newton, 2012: Internal waves on the Washington continental shelf. *Oceanography*, **25**, 66–79, doi:10.5670/oceanog.2012.43.

Bogucki, D., T. Dickey, and L. G. Redekopp, 1997: Sediment resuspension and mixing by resonantly generated internal solitary waves. *J. Phys. Oceanogr.*, **27**, 1181–1196, doi:10.1175/1520-0485(1997)027<1181:SRAMBR>2.0.CO;2.

Bourgault, D., M. D. Blokhina, R. Mirshak, and D. E. Kelley, 2007: Evolution of a shoaling internal solitary wavetrain. *Geophys. Res. Lett.*, **34**, L03601, doi:10.1029/2006GL028462.

Cummins, P. F., S. Vagle, L. Armi, and D. M. Farmer, 2003: Stratified flow over topography: Upstream influence and generation of nonlinear internal waves. *Proc. Roy. Soc. London*, **459A**, 1467–1487, doi:10.1098/rspa.2002.1077.

——, L. Armi, and S. Vagle, 2006: Upstream internal hydraulic jumps. *J. Phys. Oceanogr.*, **36**, 753–769, doi:10.1175/JPO2894.1.

da Silva, J. C. B., M. C. Buijsman, and J. M. Magalhaes, 2015: Internal waves on the upstream side of a large sill of the Mascarene Ridge: A comprehensive view of their generation mechanisms and evolution. *Deep-Sea Res. I*, **99**, 87–104, doi:10.1016/j.dsr.2015.01.002.

Dyer, K. R., 1998: *Estuaries: A Physical Introduction*. 2nd ed. Wiley, 210 pp.

Farmer, D. M., and J. D. Smith, 1980: Tidal interaction of stratified flow with a sill in Knight Inlet. *Deep-Sea Res.*, **27A**, 239–246, doi:10.1016/0198-0149(80)90015-1.

——, and L. Armi, 1999: The generation and trapping of solitary waves over topography. *Science*, **283**, 188–190, doi:10.1126/science.283.5399.188.

Garrett, C., P. MacCready, and P. B. Rhines, 1993: Boundary mixing and arrested Ekman layers: Rotating stratified flow near a sloping bottom. *Annu. Rev. Fluid Mech.*, **25**, 291–324, doi:10.1146/annurev.fl.25.010193.001451.

Gerkema, T., and J. T. F. Zimmerman, 1995: Generation of nonlinear internal tide and solitary waves. *J. Phys. Oceanogr.*, **25**, 1081–1094, doi:10.1175/1520-0485(1995)025<1081:GONITA>2.0.CO;2.

Gill, A. E., 1982: *Atmosphere–Ocean Dynamics*. Academic Press, 662 pp.

Helfrich, K. R., and W. K. Melville, 2006: Long nonlinear internal waves. *Annu. Rev. Fluid Mech.*, **38**, 395–425, doi:10.1146/annurev.fluid.38.050304.092129.

Holloway, P. E., 1987: Internal hydraulic jumps and solitons at a shelf break region on the Australian North West Shelf. *J. Geophys. Res.*, **92**, 5405–5416, doi:10.1029/JC092iC05p05405.

Hosegood, P., and H. van Haren, 2004: Near-bed solibores over the continental slope in the Faeroe-Shetland Channel. *Deep-Sea Res. II*, **51**, 2943–2971, doi:10.1016/j.dsr2.2004.09.016.

Huijts, K. M. H., H. M. Schuttelaars, H. E. de Swart, and C. T. Friedrichs, 2009: Analytical study of the transverse distribution of along-channel and transverse residual flows in tidal estuaries. *Cont. Shelf Res.*, **29**, 89–100, doi:10.1016/j.csr.2007.09.007.

Jackson, C., J. da Silva, and G. Jeans, 2012: The generation of nonlinear internal waves. *Oceanography*, **25** (2), 108–123, doi:10.5670/oceanog.2012.46.

Klymak, J. M., and J. N. Moum, 2003: Internal solitary waves of elevation advancing on a shoaling shelf. *Geophys. Res. Lett.*, **30**, 2045, doi:10.1029/2003GL017706.

Lerczak, J. A., and W. R. Geyer, 2004: Modeling the lateral circulation in straight, stratified estuaries. *J. Phys. Oceanogr.*, **34**, 1410–1428, doi:10.1175/1520-0485(2004)034<1410:MTLCIS>2.0.CO;2.

Li, M., P. Cheng, R. Chant, A. Valle-Levinson, and K. Arnott, 2014: Analysis of vortex dynamics of lateral circulation in a straight tidal estuary. *J. Phys. Oceanogr.*, **44**, 2779–2795, doi:10.1175/JPO-D-13-0212.1.

MacKinnon, J. A., and M. C. Gregg, 2003: Mixing on the late-summer New England Shelf—Solibores, shear, and stratification. *J. Phys. Oceanogr.*, **33**, 1476–1492, doi:10.1175/1520-0485(2003)033<1476:MOTLNE>2.0.CO;2.

Martin, W., P. MacCready, and R. Dewey, 2005: Boundary layer forcing of a semidiurnal, cross-channel seiche. *J. Phys. Oceanogr.*, **35**, 1518–1537, doi:10.1175/JPO2778.1.

Maxworthy, T., 1979: A note on the internal solitary waves produced by tidal flow over a three-dimensional ridge. *J. Geophys. Res.*, **84**, 338–346, doi:10.1029/JC084iC01p00338.

Melville, W. K., and K. R. Helfrich, 1987: Transcritical two-layer flow over topography. *J. Fluid Mech.*, **178**, 31–52, doi:10.1017/S0022112087001101.

Mirshak, R., and D. E. Kelley, 2009: Inferring propagation direction of nonlinear internal waves in a vertically sheared background flow. *J. Atmos. Oceanic Technol.*, **26**, 615–625, doi:10.1175/2008JTECHO632.1.

Moum, J. N., D. M. Farmer, W. D. Smyth, L. Armi, and S. Vagle, 2003: Structure and generation of turbulence at interfaces strained by internal solitary waves propagating shoreward over the continental shelf. *J. Phys. Oceanogr.*, **33**, 2093–2112, doi:10.1175/1520-0485(2003)033<2093:SAGOTA>2.0.CO;2.

Nunes, R., and J. Simpson, 1985: Axial convergence in a well-mixed estuary. *Estuar. Coast. Shelf Sci.*, **20**, 637–649, doi:10.1016/0272-7714(85)90112-X.

Omand, M. M., J. J. Leichter, P. J. S. Franks, A. J. Lucas, R. T. Guza, and F. Feddersen, 2011: Physical and biological processes underlying the sudden appearance of a red-tide surface patch in the nearshore. *Limnol. Oceanogr.*, **56**, 787–801, doi:10.4319/lo.2011.56.3.0787.

Pineda, J., 1991: Predictable upwelling and the shoreward transport of planktonic larvae by internal tidal bores. *Science*, **253**, 548–549, doi:10.1126/science.253.5019.548.

Scotti, A., R. C. Beardsley, and B. Butman, 2007: Generation and propagation of nonlinear internal waves in Massachusetts Bay. *J. Geophys. Res.*, **112**, C10001, doi:10.1029/2007JC004313.

Scully, M. E., W. R. Geyer, and J. A. Lerczak, 2009: The influence of lateral advection on the residual estuarine circulation: A numerical modeling study of the Hudson River estuary. *J. Phys. Oceanogr.*, **39**, 107–124, doi:10.1175/2008JPO3952.1.

——, A. W. Fisher, S. E. Suttles, L. P. Sanford, and W. C. Boicourt, 2015: Characterization and modulation of Langmuir circulation in Chesapeake Bay. *J. Phys. Oceanogr.*, **45**, 2621–2639, doi:10.1175/JPO-D-14-0239.1.

Wang, D., 2006: Tidally generated internal waves in partially mixed estuaries. *Cont. Shelf Res.*, **26**, 1469–1480, doi:10.1016/j.csr.2006.02.015.

Xie, X.-H., Y. Cuypers, P. Bouruet-Aubertot, A. Pichon, A. Lourenço, and B. Ferron, 2015: Generation and propagation of internal tides and solitary waves at the shelf edge of the Bay of Biscay. *J. Geophys. Res. Oceans*, **120**, 6603–6621, doi:10.1002/2015JC010827.

——, M. Li, and W. C. Boicourt, 2017: Baroclinic effects on wind-driven lateral circulation in Chesapeake Bay. *J. Phys. Oceanogr.*, **47**, 433–445, doi:10.1175/JPO-D-15-0233.1.